

Theoretical and Experimental Studies of Diffraction on Optical Disks

Yong-Wook Kim*

Korean Minjok Leadership Academy

November 8, 2023

Abstract

Incident light on an optical disk produces a distinct bright line on its surface, with the line's characteristics influenced by the relative orientations of the light source, the optical disk, and the observer. While this phenomenon is commonly discussed in many optics courses, prior research presents incorrect underlying principles. This study employs the Fraunhofer diffraction framework to investigate the underlying physics of the observed single line and to precisely quantify its position, color, and geometry. The developed theoretical model demonstrates excellent agreement with experimental data from both spectrometry and color comparisons between digitally reproduced simulations and directly observed colors. Furthermore, an additional class of line resulting from an alternative mechanism, side incidence, is introduced. The additional line's physical principles are also validated and show great consistency with directly observed colors.

*Electronic address: yongwook1124@gmail.com

Contents

1	Introduction	3
2	Microstructure of Optical Disks	3
3	Theoretical Analysis	4
3.1	Coordinate System	4
3.2	Colored Line	5
3.3	Comment on the Spectral Power Distribution	6
3.4	Comment on the Position of the Line	7
4	Experiments	7
4.1	Setup	7
4.2	Position of the Colored Line	8
4.3	Spectrometry of the Colored Line	9
4.4	Mechanism of converting spectral data to color	10
4.5	Visualization of the Colored Line	11
5	Line due to Diffraction via Side Incidence	15
5.1	Qualitative Verification	15
5.2	Quantitative Verification	17
6	Conclusion	19
7	Acknowledgements	20
A	Refractive Index of Polycarbonate Layer	21
B	Derivation of ΔOPL	21
C	Representing Track and Land as Convolutions	21
D	Computing the Fourier Integral for Simple Diffraction	22

1 Introduction

Diffraction by a CD or a DVD is a common phenomenon easily encountered during everyday experience. Moreover, this quintessential example of the diffraction phenomenon almost always makes it to the first few examples discussed in any optics course dealing with diffraction. I was first introduced to this ubiquitous yet interesting phenomenon while working on the fourth problem of the 2023 International Young Physicists' Tournament[1] as a part of the Korean National Team in the online counterpart of the competition.



Figure 1: Clear lines are visible when the line from a filament lamp is incident on the surface of optical disks. On the left is the phenomenon observed on a CD, and on the right is a DVD.

A common misconception is held about the position of the line. A paper published by De Luca et al.[3] argues that the line forms at the angle bisector between the light source and the observer due to a reflection that occurs in the direction parallel to the alignment of the grating. However, this argument is flawed, as simple diffraction does not happen in the direction parallel to the grid. Three components to the wave vector are incident on a diffraction grating: the parallel component, the perpendicular component, and the normal component. During the diffraction process, while the parallel component of the wave vector is not altered, the perpendicular component of the wave vector is added by an integer multiple of the grating vector. The dispersion relation then necessitates the normal component of the wave vector to alter, resulting in a more complicated reflection dependent on the diffraction order.

Calculating the position of the line, therefore, requires the consideration of this nontrivial reflection that occurs in the direction parallel to the gratings. The result is that the line takes the shape of a curve, whose geometry and position are dependent on many parameters, i.e., the distance of the observer from the disk, the distance of the light source from the disk, and the angles the source and the observer make with the disk.

Moreover, while an abundance of literature deals with the easy-to-observe line that is the consequence of the data tracks on the CD acting as a diffraction grating, no literature, to my knowledge, has discussed the other type of lines that are visible on a CD - one that is caused by incidence through the sides of the disk. Therefore, this paper aims to introduce this additional category of line, and to eliminate the common misconception about the more widely known class of colored line.

2 Microstructure of Optical Disks

A standard CD is comprised of four distinct layers, the foremost two are the most important in understanding the diffraction phenomenon. The first layer, the polycarbonate cover layer, is mainly transparent and has a refractive index of approximately 1.6 (see appendix A for more detailed information on the refractive index of the polycarbonate layer). The second is the data layer, which is largely reflective. The primary material used throughout the industry is aluminum, which is very reflective in the visible spectrum.

When the data layer is zoomed onto, one notices the regular pattern: concentric data tracks are positioned with a constant pitch of $1.6\mu\text{m}$, width of $0.6\mu\text{m}$, and height of approximately 110nm (There seems to be a disagreement on the width of the tracks among different sources, with some claiming 500nm and other 600nm . However, this difference of 100nm does not render a significant difference in the resulting diffraction envelope). By these properties of optical disks, CDs and DVDs act as reflective diffraction grating and synthesize various colors by various angle conditions.

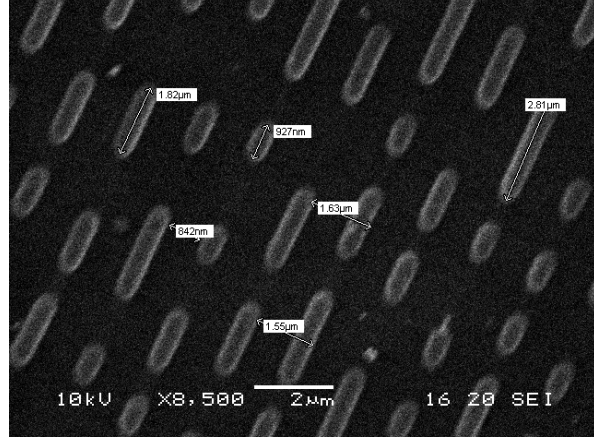


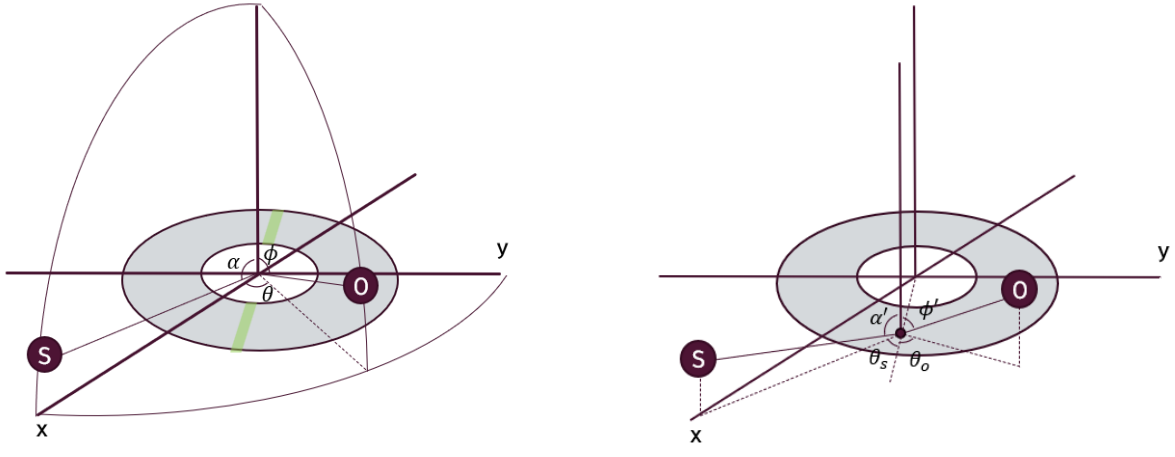
Figure 2: Micrograph of a CD-ROM made with an atomic force microscope [2].

3 Theoretical Analysis

3.1 Coordinate System

A point source and a point observer had been assumed for simplicity of calculations. To account for the consequences of physical dimensions, one needs to integrate the same effect hereafter calculated over all of the points in the physical volume.

The spherical coordinate system, where the disk is placed on the xy -plane, and the light source at $S(r_s, 0, \alpha)$, and the observer at $O(r_o, \theta, \phi)$ had been set. This way, the combination of the angles α, θ, ϕ can represent all possible orientations between the source, observer, and the disk.



(a) Coordinate System. O represents the observer, and S represents the light source.

(b) New set of angles concerning a point P on the disk.

Figure 3: Coordinate system used and the local geometry.

The calculations hereafter presumes the focus on a particular point $P = (r_p \cos \theta_p, r_p \sin \theta_p, 0)$ on

the disk's surface. Concerning this point, a new set of angles $\alpha', \phi', \theta_o, \theta_s$ had been defined to denote the relative positions of the source and the observer.

These can be easily calculated through geometry:

$$\left\{ \begin{array}{l} \tan \alpha' = \frac{r_s \cos \alpha}{\sqrt{(r_s \sin \alpha - r_p \cos \theta_p)^2 + r_p^2 \sin^2 \theta_p}} \\ \tan \phi' = \frac{r_o \cos \phi}{\sqrt{(r_o \sin \phi \cos \theta - r_p \cos \theta_p)^2 + (r_o \sin \phi \sin \theta - r_p \sin \theta_p)^2}} \\ \theta_o + \theta_s = \theta' \\ \theta' = \tan^{-1} \left(\frac{r_o \sin \phi \sin \theta - r_p \sin \theta_p}{r_o \sin \phi \cos \theta - r_p \cos \theta_p} \right) - \tan^{-1} \left(\frac{-r_p \sin \theta_p}{r_s \sin \alpha - r_p \cos \theta_p} \right) \\ \theta_p - \theta_s = \tan^{-1} \left(\frac{-r_p \sin \theta_p}{r_s \sin \alpha - r_p \cos \theta_p} \right) \end{array} \right. \quad (1)$$

Notice that if the range of the \tan^{-1} functions in the 4th equation were limited to the usual range of $(-\frac{\pi}{2}, \frac{\pi}{2})$, the line would appear on only half of the CD. Thus, an additional term of π must be added to the equation should one wish to calculate the position of the line on the other half of the CD as well.

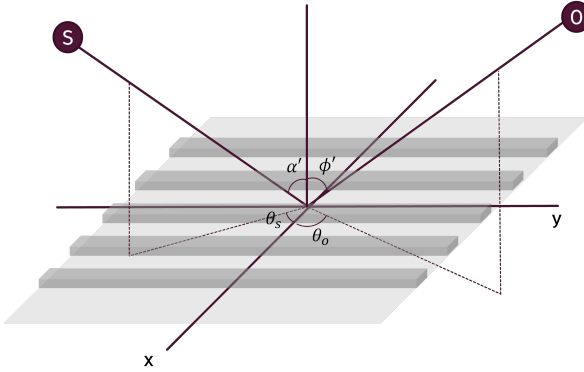


Figure 4: A schematic diagram of the zoomed-in surface of an optical disk. The protruding darker gray boxes represent the data tracks and the flat grey regions in between the lands. Notice that the xy axes have been redefined from figure 3 so that the new x-axis passes through the origin and point P .

When this local view is considered, all incident and reflected rays can be approximated to be parallel to themselves since the effect from the wavefront curvature is negligible compared to the wavelength of visible light when only a handful of grating patterns are considered. Therefore, the linear framework of Fraunhofer diffraction can and will be used throughout the following theoretical calculations.

3.2 Colored Line

We first consider the case where the incident rays are entering the polycarbonate cover layer through incidence at the top.

Two causes lead to optical path differences between parallel incident rays. The first cause of such optical path difference is the horizontal separation between light rays. Rays incident on the CD will all be first refracted, reflected off the data layer, and again refracted out to arrive at the observer. The optical path difference that occurs in this process with the horizontal separation $\vec{r}' = (x, y, 0)$ is

$$-ik (\sin \alpha' \cos \theta_s + \sin \phi' \cos \theta_o) x - ik (\sin \phi' \sin \theta_o - \sin \alpha' \sin \theta_s) y \quad (2)$$

where $k = \frac{2\pi}{\lambda}$ is the wavenumber. Abbreviations of $\widetilde{k}_x = k (\sin \alpha' \cos \theta_s + \sin \phi' \cos \theta_o)$ and $\widetilde{k}_y = k (\sin \phi' \sin \theta_o - \sin \alpha' \sin \theta_s)$ are used to denote the phase difference in the complex amplitude succinctly:

$$e^{-i(\widetilde{k}_x x + \widetilde{k}_y y)} \quad (3)$$

Another cause of optical path difference is that some light reflects off on the tracks, while others reflect off the lands between the tracks. The optical path difference that occurs in this manner can be geometrically calculated as:

$$\Delta OPL = \frac{h}{n_{pc}} \left(\sqrt{n_{pc}^2 - \sin^2 \alpha'} + \sqrt{n_{pc}^2 - \sin^2 \phi'} \right) \quad (4)$$

See appendix B for a detailed derivation. This rather long expression will be denoted by ΔOPL hereafter. This also causes a phase difference in the complex amplitude of light rays.

A sum of rectangle functions about the x-axis (see figure 4) is used to characterize the tracks and the lands. The following definition of the rectangle function has been used throughout the paper.

$$\text{rect}(x, w) = \begin{cases} 1, & -\frac{w}{2} \leq x \leq \frac{w}{2} \\ 0, & x < -\frac{w}{2} \text{ or } x > \frac{w}{2} \end{cases} \quad (5)$$

The sum had been expressed as a convolution for a more straightforward computation of the Fourier integral later (see appendix C for a detailed explanation).

$$\left\{ \begin{array}{l} \text{track} = \text{rect}(x, w) * \sum_{n=-\frac{N}{2}}^{\frac{N}{2}-1} \delta(x - n\Lambda) \\ \text{land} = \text{rect}(x, \Lambda - w) * \sum_{n=-\frac{N}{2}}^{\frac{N}{2}-1} \delta(x - n\Lambda - \frac{\Lambda}{2}) \end{array} \right. \quad (6)$$

The complex amplitude of observed light has two components: one diffracted from the top of the data tracks and one diffracted from the lands between data tracks. These two contributions are linearly combined to compose the total complex amplitude observed by the observer:

$$U = U_o \iint_{\text{track}} e^{-i(\widetilde{k_x}x + \widetilde{k_y}y)} dx dy + U_o e^{in_{pc}k\Delta OPL} \iint_{\text{land}} e^{-i(\widetilde{k_x}x + \widetilde{k_y}y)} dx dy \quad (7)$$

The integral is equivalent to a 2D Fourier Transform. Using the convolution theorem, the integral may be easily computed. Using the fact that the intensity of light is the complex amplitude multiplied by its complex conjugate ($I = U\bar{U}$), the observed intensity takes the form of:

$$I = I_o \frac{\sin^2\left(\frac{N}{2}\widetilde{k_x}\Lambda\right)}{\sin^2\left(\frac{1}{2}\widetilde{k_x}\Lambda\right)} D(\alpha', \phi', \theta_o, \theta_s) \delta(\widetilde{k_y}) \quad (8)$$

with

$$\begin{aligned} D(\alpha', \phi', \theta_o, \theta_s) = & w^2 \text{sinc}^2\left(\frac{1}{2}\widetilde{k_x}w\right) + (\Lambda - w)^2 \text{sinc}^2\left(\frac{1}{2}\widetilde{k_x}(\Lambda - w)\right) \\ & + 2w(\Lambda - w) \text{sinc}^2\left(\frac{1}{2}\widetilde{k_x}w\right) \text{sinc}^2\left(\frac{1}{2}\widetilde{k_x}(\Lambda - w)\right) \cos\left(\frac{1}{2}\widetilde{k_x}\Lambda - n_{pc}k\Delta OPL\right) \end{aligned} \quad (9)$$

This formula underlies the primary line that is the artifact of simple diffraction. You may refer to appendix D for derivation.

3.3 Comment on the Spectral Power Distribution

As in equation 8, the spectral power distribution of observed light depends on three terms: namely, the initial spectral power distribution, interference pattern, and diffraction envelope. The initial spectral power distribution (I_o) is that from the filament lamp itself. It was measured with a spectrometer in a controlled environment with suppressed lighting, and takes the shape of figure 5.

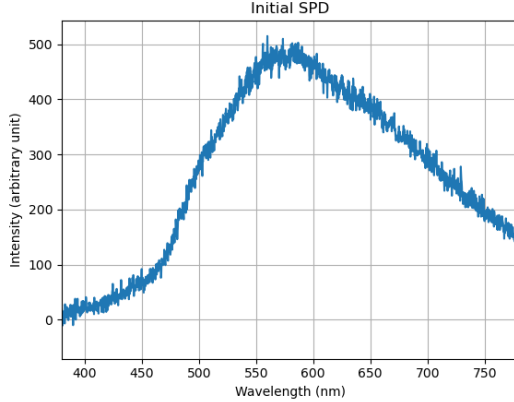


Figure 5: Initial Spectral Power Distribution of the filament lamp.

The second term $\left(\frac{\sin^2\left(\frac{N}{2}\widetilde{k_x}\Lambda\right)}{\sin^2\left(\frac{1}{2}\widetilde{k_x}\Lambda\right)} \right)$ denotes the interference pattern of the observed intensity. It shows peaking behavior at points where $\frac{1}{2}\Lambda\widetilde{k_x} = m\pi$, where m is an integer. From this, the wavelengths at which maxima in intensity occur can be computed for every point on the line. Third, the diffraction envelope $D(\alpha', \phi', \theta_o, \theta_s)$ encapsulates nontrivial relative intensities associated with lights of different diffraction orders.

This formula for intensity can be used to construct an intensity versus wavelength graph. The initial spectral power distribution and the diffraction envelope of the corresponding diffraction order determine the peaks' heights. This distribution is integrated with the XYZ color matching functions and converted to a single color in the XYZ color space for later simulation (see section 4.4 for a detailed explanation).

3.4 Comment on the Position of the Line

Due to the characteristic of the Dirac-delta function, the intensity will be only visible where $\widetilde{k_y} = 0$, or more simply:

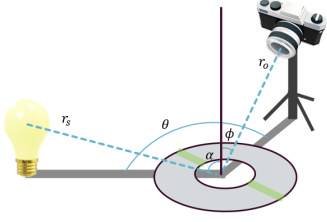
$$\sin \alpha' \sin \theta_s = \sin \phi' \sin \theta_o \quad (10)$$

This constraint will specify a single curve on the surface of the CD, which will constitute the position of the line. Notice how the above condition differs from the angle-bisector condition argued in De Luca et al's paper [3]. The paper's argument only stands when both α' and ϕ' are large enough so that both $\sin \alpha'$ and $\sin \phi'$ can be considered unity. Generally, the line does not form at the angle bisector.

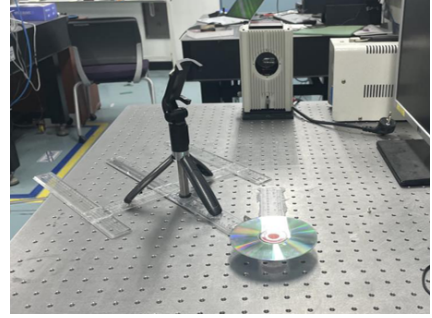
4 Experiments

4.1 Setup

A selfie rod was used to adjust the vertical position of the photosensitive device (iPhone 12 camera for color observation and UV-VIS-NIR-Spectrometer from OtO Photonics SE2060-025-VNIR for spectrometry), thus altering the angle of observation (ϕ) and the distance to the optical disk from the photosensitive device (r_o). The distance from the disk to the light source and the angle of incidence was fixed to specific values, while the azimuthal angle (θ) was varied from 15° to 180° with 5° interval using a digital protractor.



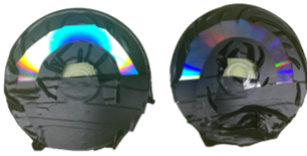
(a) A schematic diagram of the experimental setup.



(b) A photograph of the actual experimental setup.

Figure 6: Experimental setup.

For more accurate spectrometry, the optical disks were taped so that only light diffracted from the desired section (the region where $3\text{cm} < r < 5\text{cm}$) of the disks could be detected. Moreover, a polarization filter was attached to the iPhone camera to reduce the glare effect on the camera caused by the strong intensity of the diffracted line.



(a) A photograph of the taped CD(left) and DVD(right).



(b) A photograph of the polarization filter used on camera.

Figure 7: Photographs of additional measures applied to the experimental setup.

The experiments were conducted in a laboratory environment specifically designed for optics experiments by eliminating virtually all light sources.

4.2 Position of the Colored Line

First, to verify the line's position predicted by formula 10, the line was digitally simulated and copied onto physical optical disks. The optical disks were then photographed from various orientations, and the line's marked and actual positions were visually compared.

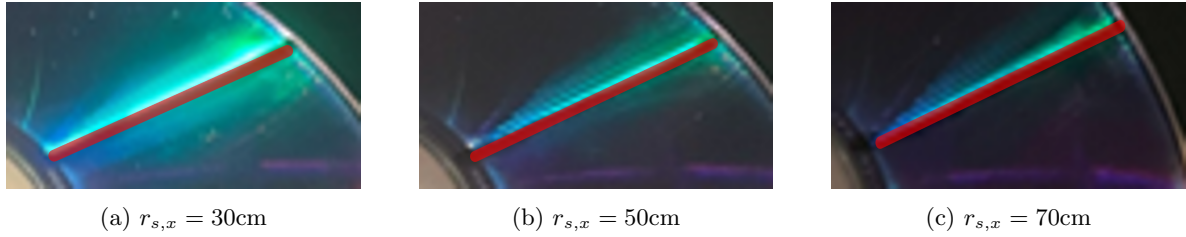


Figure 8: Photographs obtained by varying the horizontal distance between the light source and the optical disk. $\theta = 90^\circ$ For visibility, the previously marked position of the line was highlighted with a red line.

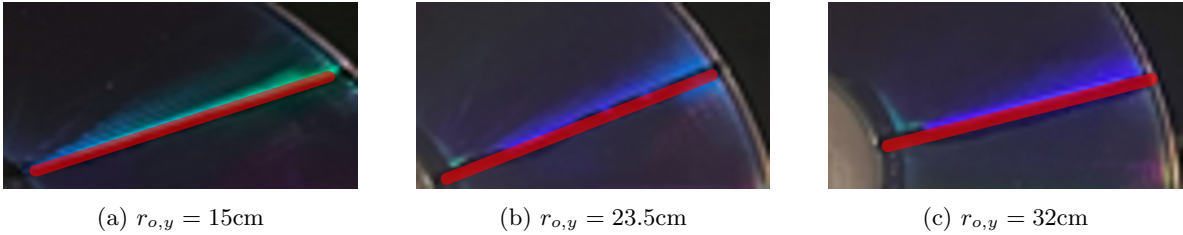


Figure 9: Photographs obtained by varying the altitude of the observer. $\theta = 90^\circ$ For visibility, the previously marked position of the line was highlighted with a red line.

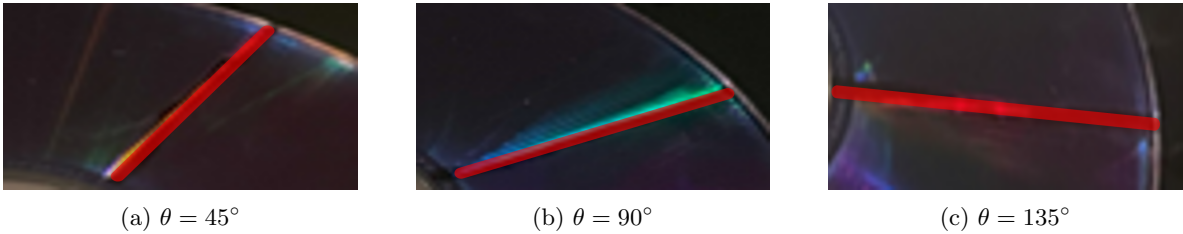


Figure 10: Photographs obtained by varying θ . The previously marked position of the line was highlighted with a red line for visibility.

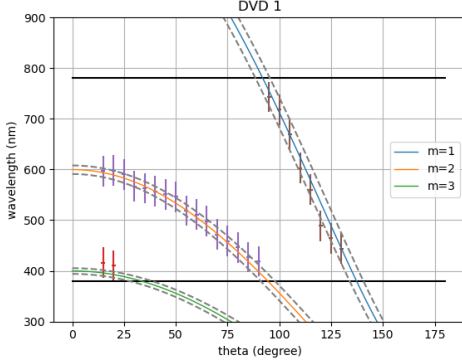
All of the observed lines virtually coincide with the theoretically predicted position. Therefore, it could be concluded that equation 10 is valid for predicting the position of the line.

4.3 Spectrometry of the Colored Line

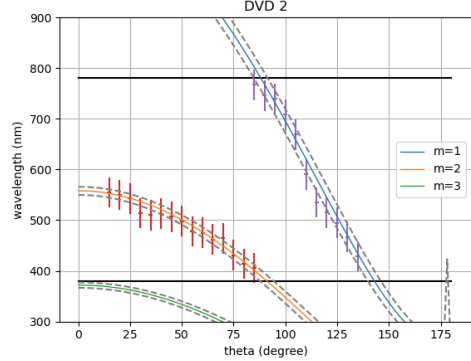
A spectrometry was conducted to verify the peak wavelengths of diffraction. To test the spectrum at as many orientations as possible, experiments were divided into 3 cases as outlined in table 1. For each case, the value of θ was varied from 15° to 180° , with a 5° increment between each step. The same experiment was repeated for an unwritten CD-R and an unwritten DVD-R.

Cases	r_o	ϕ
Case 1	29.4cm	45°
Case 2	36.6cm	36.4°
Case 3	42.6cm	29.5°

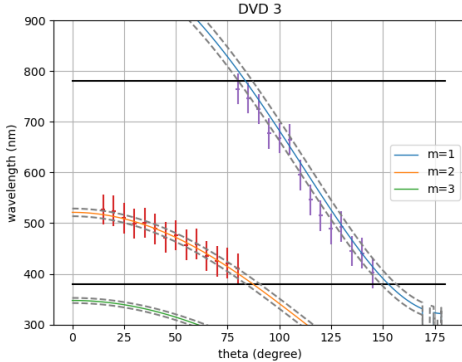
Table 1: The above table lists the setup orientations in the three experiment cases. In each, r_s had been fixed to 70.8cm, and α at 83.5° .



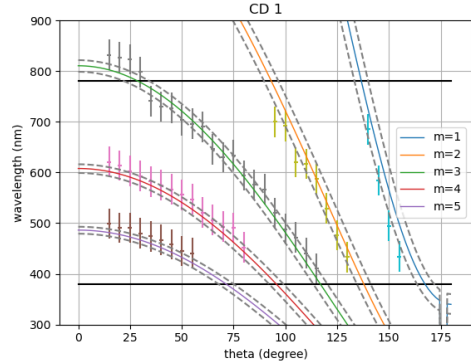
(a) Spectrometry of DVD in Case 1.



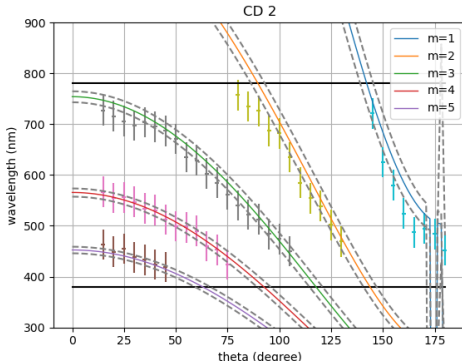
(b) Spectrometry of DVD in Case 2.



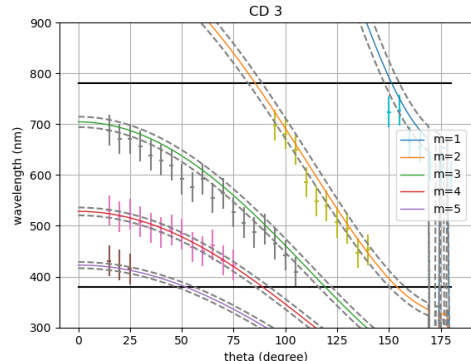
(c) Spectrometry of DVD in Case 3.



(d) Spectrometry of CD in Case 1.



(e) Spectrometry of CD in Case 2.



(f) Spectrometry of CD in Case 3.

Figure 11: Spectrometry of the DVD and the CD.

Each colored line on the graph denotes the predicted peak wavelength per θ , and the grey lines that surround each colored line represent the minimum and maximum wavelengths that are observable within this region.

The y-axis error bar on the data points reflects the error rate in wavelength measurement reported by the spectrometer manufacturer, and the x-axis error bar the uncertainty in the angle measurement of θ (approximately 1°). As the graphs show, the predicted peaks were well within the error bound, and thus equation 8 was proven valid in predicting the peak wavelengths.

4.4 Mechanism of converting spectral data to color

Although peak wavelengths and their relative intensities provide information on the observed color, color theory must be employed to predict the precise color and compare it with the observed color.

The CIE 1931 XYZ colorspace is widely used to define other colorspaces and chromaticity in general. A spectral power distribution may be converted to the XYZ colorspace by performing an integral over the visible wavelength range with the appropriate color matching functions.

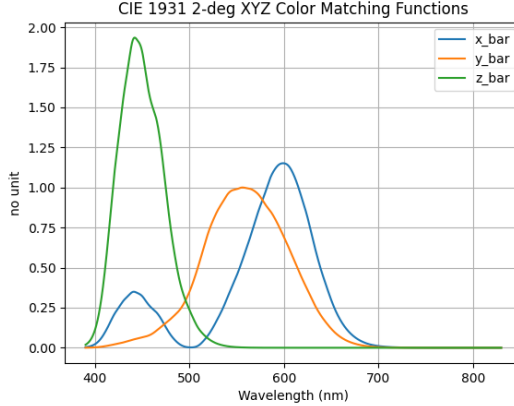


Figure 12: The CIE 1931 2-deg XYZ color matching functions were used for calculation.

$$\left\{ \begin{array}{l} X = \int_{visible} I(\lambda) \bar{x}(\lambda) d\lambda \\ Y = \int_{visible} I(\lambda) \bar{y}(\lambda) d\lambda \\ Z = \int_{visible} I(\lambda) \bar{z}(\lambda) d\lambda \end{array} \right. \quad (11)$$

Then, a standardized conversion algorithm between the CIE 1931 XYZ colorspace and sRGB colorspace may be used to visualize the calculated color digitally[5]. To convert, we utilize the linearized RGB values:

$$\begin{bmatrix} R_{linear} \\ G_{linear} \\ B_{linear} \end{bmatrix} = \begin{bmatrix} +3.2406255 & -1.5372080 & -0.4986286 \\ -0.9689307 & +1.8757561 & +0.0415175 \\ +0.0557101 & -0.2040211 & +1.0569959 \end{bmatrix} \begin{bmatrix} X \\ Y \\ Z \end{bmatrix} \quad (12)$$

The linearized RGB values are next converted into the final RGB values with the following algorithm:

$$C_{sRGB} = \begin{cases} 12.92C_{linear}, & C_{linear} \leq 0.0031308 \\ 1.055C_{linear}^{1/2.4} - 0.055, & C_{linear} > 0.0031308 \end{cases} \quad (13)$$

where C denotes any one of the three chromaticities: R , G , B . If the chromaticity values exceed the $[0, 1]$ range during any computation process, the value may be clipped to comply with the range.

4.5 Visualization of the Colored Line

A Python code was implemented to digitally reproduce the position and color of the line observed from any given orientation. The orientations of Case 1, 2, and 3 with θ values of 15° , 90° , and 165° were selected to compare the results of the simulation and the observed color. However, due to the difference in dimension between an iPhone and an optical fiber, the definitions of cases 1 through 3 had been slightly altered for this experiment.

Cases	r_o	ϕ
Case 1	23cm	38°
Case 2	30cm	29°
Case 3	35cm	23°

Table 2: The above table lists the setup orientations in the three experiment cases. Same as in table 1, r_s had been fixed to 70.8cm and α at 83.5°. Special values of θ were chosen for visual comparison - 15°, 90°, and 165°.

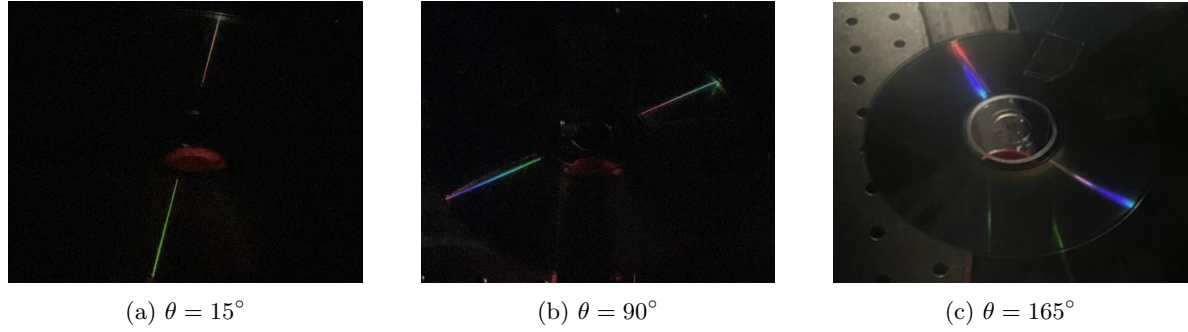


Figure 13: Photographs taken of a CD-R at Case 1 orientation and $\theta = 15^\circ, 90^\circ, 165^\circ$.

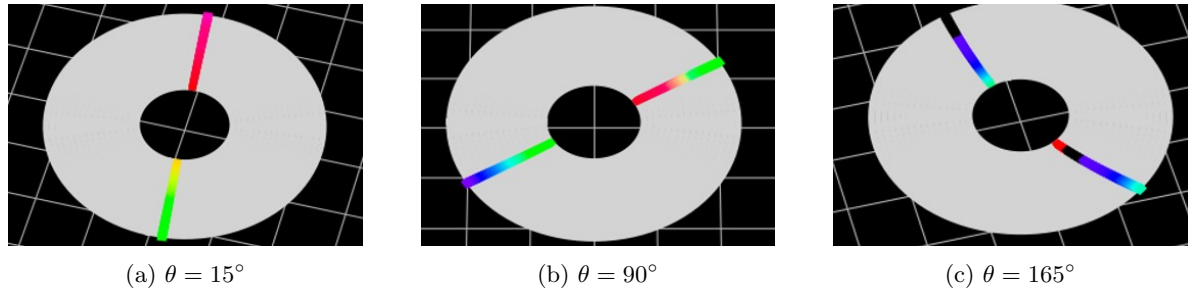


Figure 14: Simulations of a CD-R at Case 1 orientation and $\theta = 15^\circ, 90^\circ, 165^\circ$.

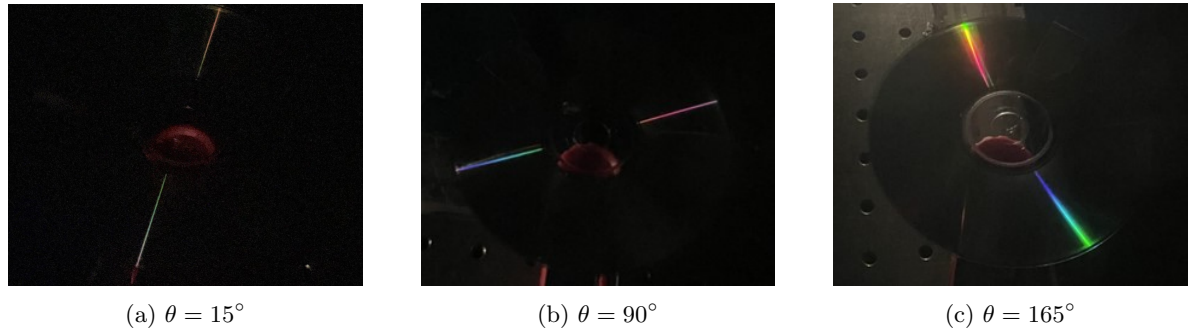


Figure 15: Photographs taken of a CD-R at Case 2 orientation and $\theta = 15^\circ, 90^\circ, 165^\circ$.

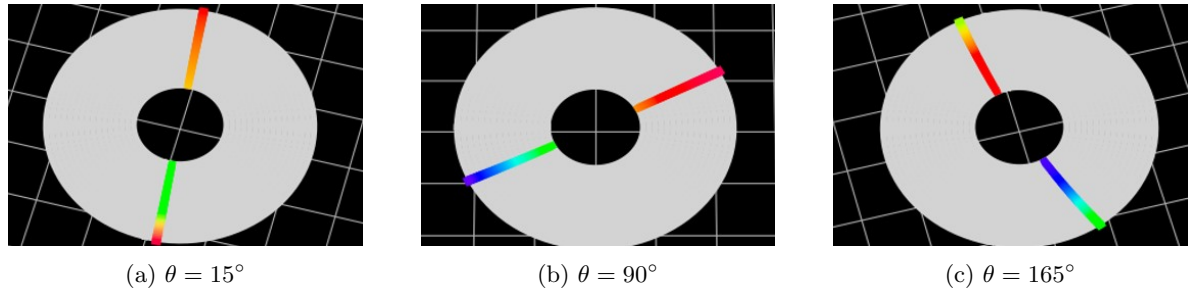


Figure 16: Simulations of a CD-R at Case 2 orientation and $\theta = 15^\circ, 90^\circ, 165^\circ$.

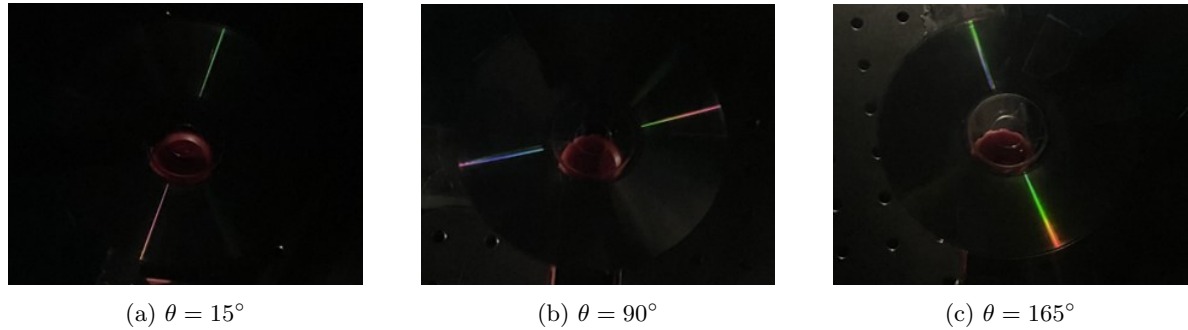


Figure 17: Photographs taken of a CD-R at Case 3 orientation and $\theta = 15^\circ, 90^\circ, 165^\circ$.

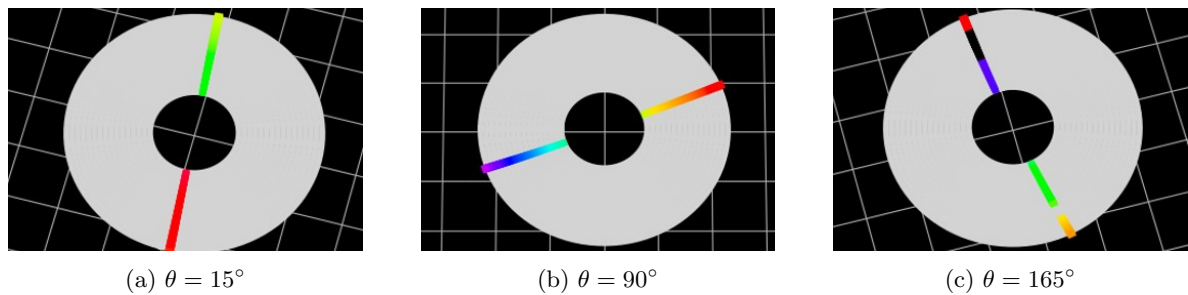


Figure 18: Simulations of a CD-R at Case 3 orientation and $\theta = 15^\circ, 90^\circ, 165^\circ$.

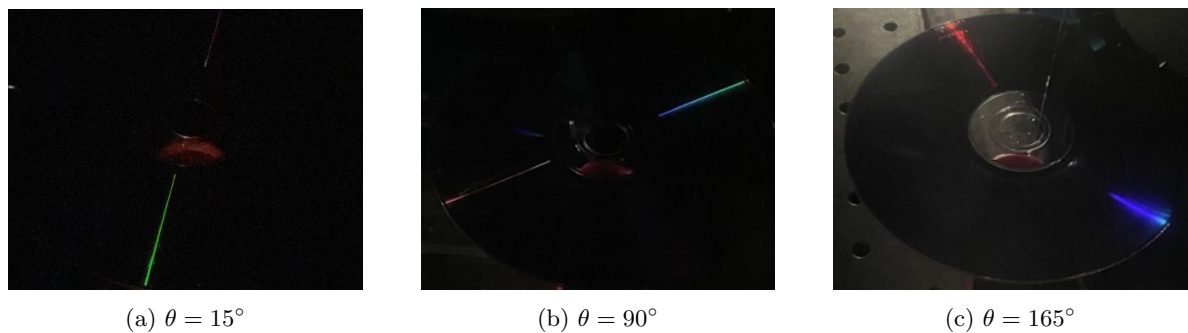


Figure 19: Photographs taken of a DVD-R at Case 1 orientation and $\theta = 15^\circ, 90^\circ, 165^\circ$.

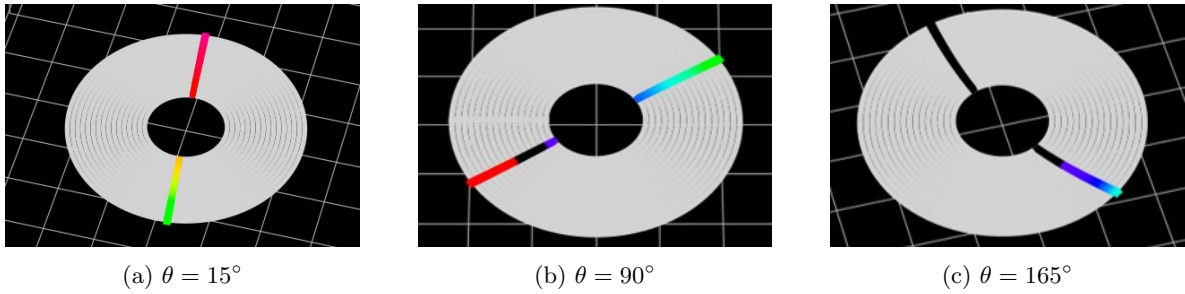


Figure 20: Simulations of a DVD-R at Case 1 orientation and $\theta = 15^\circ, 90^\circ, 165^\circ$.

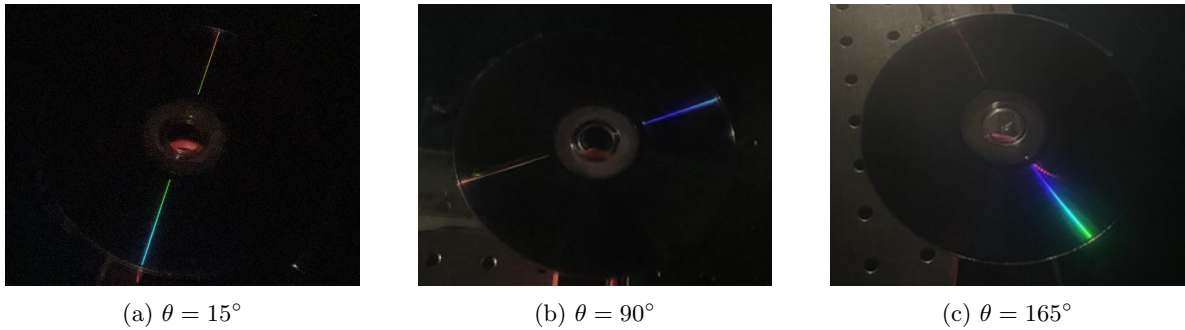


Figure 21: Photographs taken of a DVD-R at Case 2 orientation and $\theta = 15^\circ, 90^\circ, 165^\circ$.

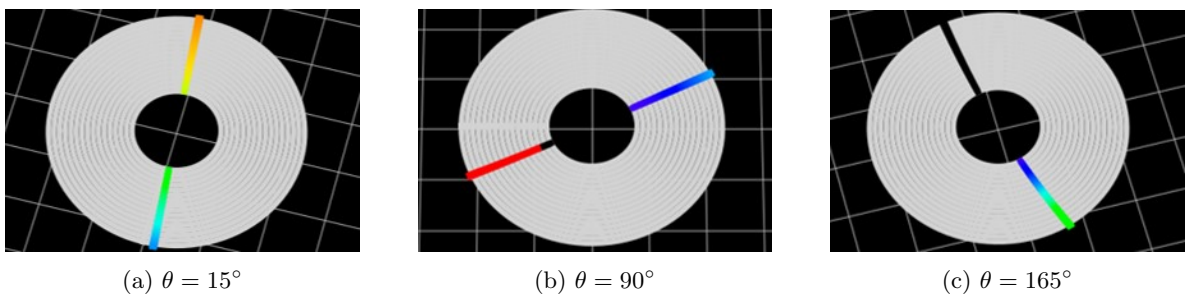


Figure 22: Simulations of a DVD-R at Case 2 orientation and $\theta = 15^\circ, 90^\circ, 165^\circ$.

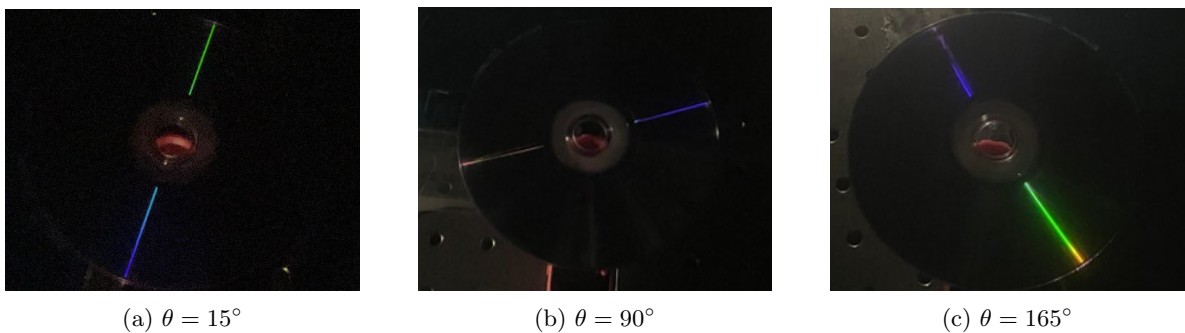


Figure 23: Photographs taken of a DVD-R at Case 3 orientation and $\theta = 15^\circ, 90^\circ, 165^\circ$.

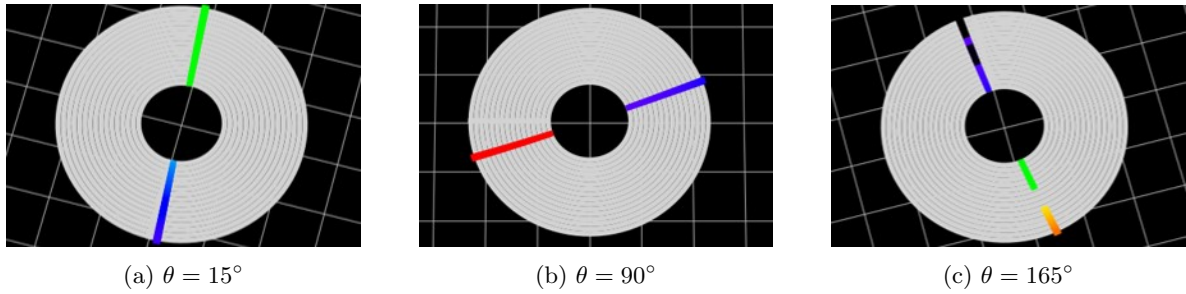


Figure 24: Simulations of a DVD-R at Case 3 orientation and $\theta = 15^\circ, 90^\circ, 165^\circ$.

Considering the sensitivity of the peak wavelength with respect to slight variations in the position of the camera, some minor error is present. Plus, because the RGB value of each pixel had been independently normalized to the range $[0, 1]$, the simulation fails to reflect the relative intensities between different sections of the line. Nevertheless, the simulated color shows great agreement with what was observed. Therefore, it could be concluded that equation 8 was successful in predicting all physical characteristics of the colored line: position, geometry, and color. While the limitation of a physical paper had restricted the comparison to the angles 15° , 90° and 165° , a video-based comparison for all values of θ (from 15° to 180°) can be found on my personal GitHub repository [6].

5 Line due to Diffraction via Side Incidence

This section introduces an additional colored line that appears as the result of a mechanism other than the simple diffraction discussed in previous sections - namely, the line that appears due to light entering the disk through the side. A regular CD has a thickness of 1.2mm. This leaves a small room for some light to enter the CD through the sides. This effect creates another line (though much weaker in intensity than the line produced by regular incidence) at a slightly different position on the disk as in figure 25, the line forms at places on the optical disk where simple diffraction cannot produce a color.

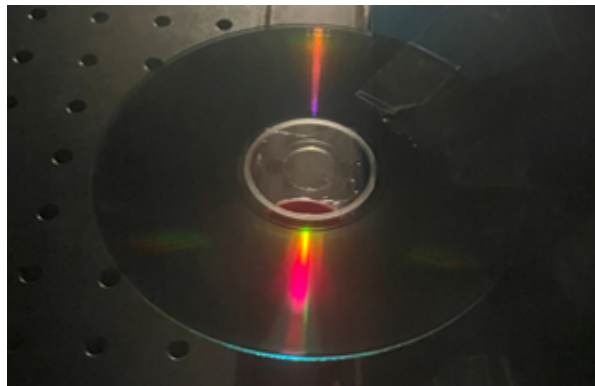


Figure 25: A demonstration of the colored line through side incidence. The rainbow on the bottom side of the disk displays the 1st-order diffraction spectrum, making the line on the upper side of the disk unaccountable by simple diffraction. The line on top is caused by incidence through the side of the optical disk.

5.1 Qualitative Verification

First, to verify that incidence through the side is indeed the cause of this additional line, an experiment was devised. A He-Ne laser ($\lambda = 632.8\text{nm}$) had been placed at the position of the light source, and shot at 1) the face, and 2) the side of the disk. In place of the camera, a white screen had been attached to visually locate the maxima of diffraction. The position where the camera would have been had been marked with a black circle.

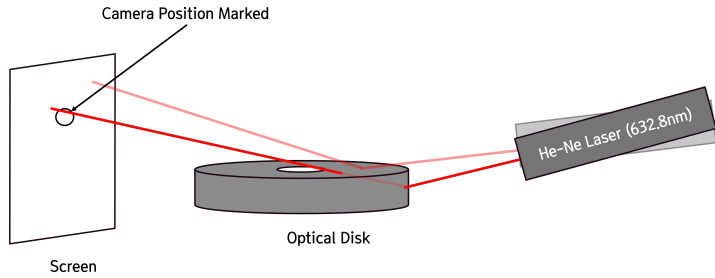
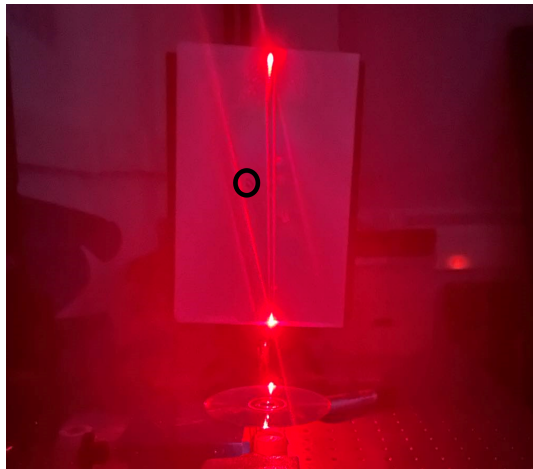
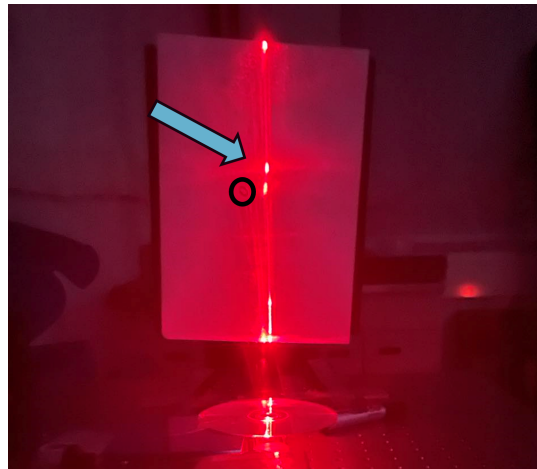


Figure 26: A schematic diagram of the laser experiment.

Below are the results of the experiments with a CD (figure 27) and DVD (figure 28). It can be clearly observed that when the laser was shot at the side, both CD and DVD created peaks around the marked position of the camera, which implies that colors of wavelengths around 632.8nm must be observable at such configurations.

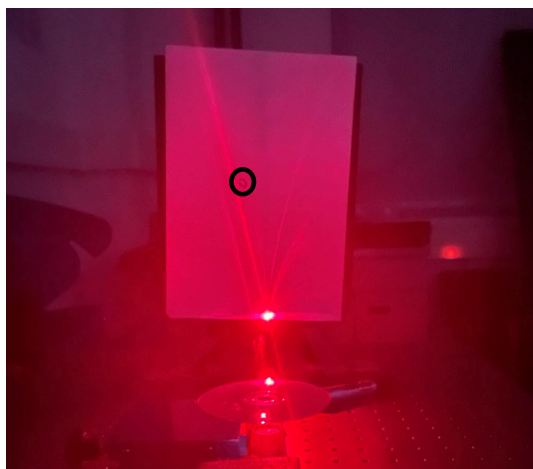


(a) Control (laser shot at the face)

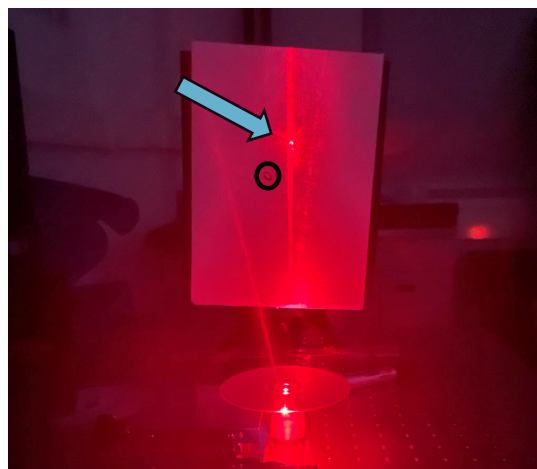


(b) Experiment (laser shot at the side)

Figure 27: A comparison between the diffraction peaks projected on a screen when the laser was aimed at the face of the CD and when it was aimed at the side of the CD.



(a) Experiment (laser shot at the surface)



(b) Color (laser shot at the side)

Figure 28: A comparison between the diffraction peaks projected on a screen when the laser was aimed at the face of the DVD and when it was aimed at the side of the DVD.

As noticeable in figures 32a and 33a, the regions on both CD and DVD where the light from the filament lamp had penetrated from the side emanate in orange colors, which indeed have wavelengths around 600nm. Thus, it had been confirmed that incidence through the side creates new peaks, and that these peaks are responsible for the additional line that appears on the disk, where no simple diffraction can produce visible color.

5.2 Quantitative Verification

Next, a simple quantitative model was employed to predict the colors that side incidence produces. A slightly different geometry should be considered to account for the refraction that occurs at the side of the disk. For simplicity of calculation, and since the main aim of this section is to provide an introductory explanation rather than an extensive study, we consider the special case of $\theta = 180^\circ$, where the entire system can be collapsed to a single plane.

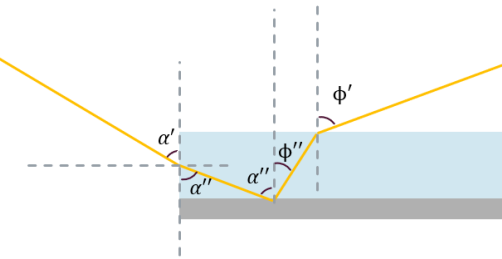


Figure 29: A schematic diagram of side incidence at $\theta = 180^\circ$.

α' and ϕ' are simply found by the following depending on the side (far or near) of the disk considered.

$$\begin{cases} \tan \alpha' = \frac{r_{s,x} - r_{out}(\text{or } +r_{in})}{r_{s,z}} \\ \tan \phi' = \frac{r_{o,x} + r_{out}(\text{or } -r_{in}) - r}{r_{o,z}} \end{cases} \quad (14)$$

r_{out} is the outer radius of the disk (6cm), and r_{in} the inner radius(2cm). By Snell's Law, it is evident that $\cos \alpha' = n_{pc} \cos \alpha''$ and $\sin \phi' = n_{pc} \sin \phi''$. We write the same integral as equation 7 for the complex amplitude of observed light, but ignoring the y-component thanks to the planar geometry considered.

$$U = U_o \iint_{\text{track}} e^{-i\tilde{k}x} dx + U_o e^{in_{pc}k\Delta OPL} \iint_{\text{land}} e^{-i\tilde{k}x} dx \quad (15)$$

Here, $\tilde{k} = n_{pc}k (\sin \phi'' - \sin \alpha'')$. Similarly to section 3.2, calculating $I = U\bar{U}$ yields

$$I = I_o \frac{\sin^2 \left(\frac{N\tilde{k}\Lambda}{2} \right)}{\sin^2 \left(\frac{1}{2}\tilde{k}\Lambda \right)} D(\alpha'', \phi'') \quad (16)$$

where

$$\begin{aligned} D(\alpha'', \phi'') = & w^2 \operatorname{sinc}^2 \left(\tilde{k} \frac{w}{2} \right) + (\Lambda - w)^2 \operatorname{sinc}^2 \left(\tilde{k} \frac{(\Lambda - w)}{2} \right) \\ & + 2w(\Lambda - w) \operatorname{sinc} \left(\tilde{k} \frac{w}{2} \right) \operatorname{sinc} \left(\tilde{k} \frac{(\Lambda - w)}{2} \right) \cos \left(\tilde{k} \frac{\Lambda}{2} - n_{pc}k\Delta OPL \right) \end{aligned} \quad (17)$$



Figure 30: A photograph of the fringe-like pattern of the side-incidence line. You can clearly see the fringe-like consecutive peaks on the upper half of the disk. The lower portion of the disk's center was covered with black tape so that rays that entered through a small protruding structure were filtered, leaving only the rays that entered through the side to be detected by the camera.

Due to the high refractive index of the polycarbonate cover layer and the limited thickness of the disk, however, the line exhibits a different pattern than the simply diffracted line. The incident rays, due to their large angles in the polycarbonate, cannot escape unless diffracted by the grating. Thus, a fringe-like pattern is created whereby a sequence of regions where light is diffracted and regions where light is not diffracted and undergoes total internal reflection is visible instead of a single continuous line.

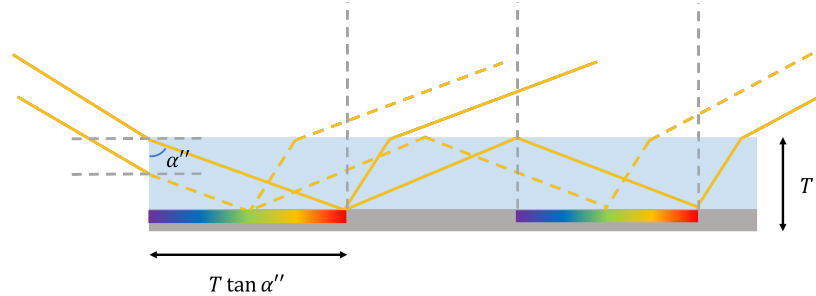


Figure 31: A schematic diagram of the total internal reflection inside the polycarbonate cover layer, which creates fringe-like patterns. The regions where light would be visible had been denoted with a rainbow, while regions where light would not be visible is left grey.

The length of each individual strip of color/darkness is calculated as on the figure to be $T \tan \alpha''$. With this incorporated, a similar Python code as 4.5 was implemented to simulate the side-incidence line observed at $\theta = 180^\circ$ and to test the validity of equation 16.

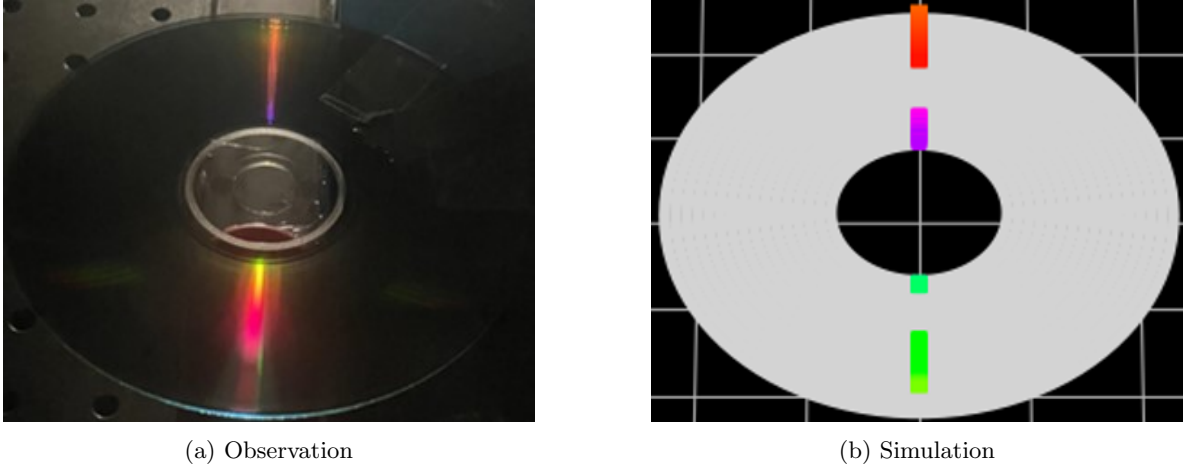


Figure 32: Comparison between the observation and the simulation of CD at Case 1 orientation. $\theta = 180^\circ$. You can see that the orange and violet strips at the top of the observed photograph match the orange color at the top of the simulated CD. Moreover, the green, although mostly covered by the first-order spectrum, on the lower side of the CD in the photograph matches that of the simulation.

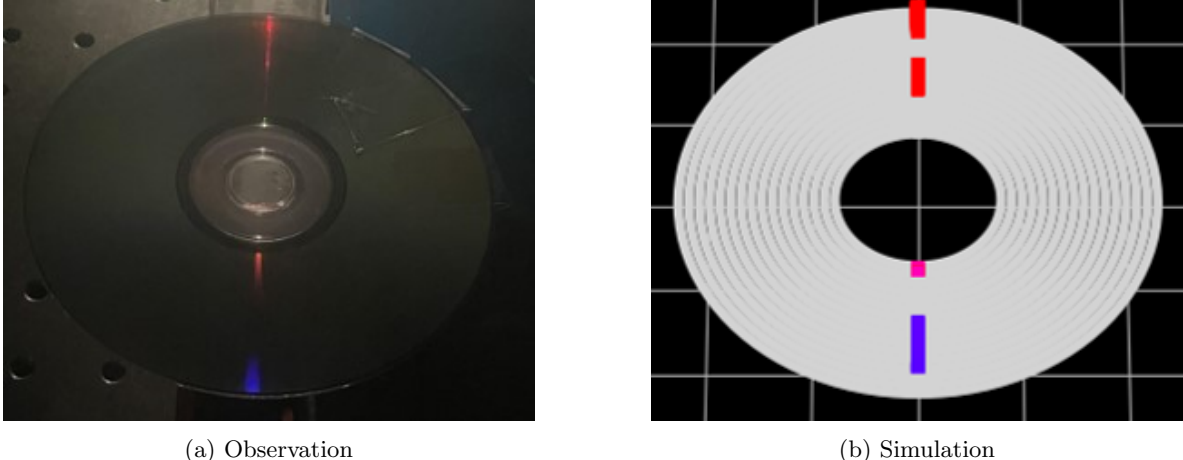


Figure 33: Comparison between the observation and the simulation of DVD at Case 1 orientation. $\theta = 180^\circ$. It can be seen that the two red peaks on top of the CD had been accurately simulated. The blue trail at the bottom of the observed photograph is the tail of the first-order diffraction spectrum, and the purple strip on the lower side of the simulation represents a very weak peak of $\lambda \approx 410\text{nm}$, which should not have been captured by the camera both because of its weak intensity and the camera's low sensitivity to wavelengths around 400nm.

Only the pictures of the CD and DVD at case 1 orientation were compared, since the smaller the value of ϕ' , the harder it becomes to observe the side-diffraction line due to the relative brightness of the main diffraction line. However, the simulation seems to agree well with the observed color in both cases.

6 Conclusion

First, this paper elucidated the physical causes that create a single colored line on the surface of an optical disk when light is incident. It occurs due to the $\delta(\tilde{k}_y)$ term that appears upon computing the Fraunhofer diffraction formula, which makes the observed intensity vanish everywhere except where $\tilde{k}_y = 0$, or $\sin(\alpha') \sin(\theta_s) = \sin(\phi') \sin(\theta_o)$. This geometrical constraint necessitates that only one line

be observed by the observer, and the position of the line predicted by this formula had been verified experimentally to be exactly where the colored line forms.

Second, this paper clarified two causes of optical path differences between parallel light rays: the horizontal separation between incident rays and where the ray is reflected from (the track or the land). While only considering the horizontal separation can predict the same peaking behavior of wavelengths, the second cause of optical path difference introduces an extra interference that results in a nontrivial diffraction envelope. This is responsible for the weighted combination of peak wavelengths that synthesize various colors at various orientations. Plus, both the spectrometry experiment, testing for peak wavelengths, and direct color comparison (which can be found on my personal GitHub repository [6]) showed excellent agreement with the developed theoretical model, which testifies to the validity of the theoretical arguments of the paper.

Lastly, the paper introduced an additional line due to side incidence that had not been reported in the literature and proposed qualitative and quantitative explanations. The light incident through the side can create a line where no simple diffraction can be accounted for and shows a fringe-like behavior due to the large refractive index of the polycarbonate layer as well as the large angle of incidence.

Optical disks, such as CDs and DVDs, are objects one encounters often in everyday life. Moreover, it is often introduced as a quintessential example of a diffraction grating in many introductory optics courses and textbooks. However, while De Luca[3] and other researchers have successfully predicted and explained the color of the line in limited circumstances, a generally valid theoretical investigation into the phenomenon has not yet been conducted to the author's knowledge. Therefore, the significance of this research lies in correcting misconceptions present in the current literature and providing a thorough mathematical representation of the various colors produced on a disk.

7 Acknowledgements

I thank the 2023 Online Young Physicists' Tournament Team Korea members for the wonderful month in preparation for the tournament. I also express modest gratitude to Mr. Yeounsoo Kim, who supervised our school team participating in the 2023 Korean Young Physicists Tournament and Mr. Claire Byeon, who gave me invaluable feedback while preparing for the international competition.

References

- [1] IYPT International Organising Committee(IOC). *Problems for the 36th IYPT 2023*. 2022. URL: <https://www.iypt.org/problems/problems-for-the-36th-iypt-2023/>.
- [2] Wikimedia Commons. *Picture of a CD from a Scanning Electron Microscopy*. 2006. URL: https://commons.wikimedia.org/wiki/File:Cd_MEB.jpg.
- [3] R. De Luca et al. "A compact disc under skimming light rays". In: *American Journal of Physics* 86.3 (Mar. 2018), pp. 169–173. ISSN: 0002-9505. DOI: [10.1119/1.5021904](https://doi.org/10.1119/1.5021904).
- [4] J.W. Goodman. *Introduction to Fourier Optics*. Electrical Engineering Series. McGraw-Hill, 1996. ISBN: 9780070242548.
- [5] International Electrotechnical Commission. *Amendment 1 - Multimedia systems and equipment - Colour measurement and management - Part 2-1: Colour management - Default RGB colour space - sRGB*. en. Standard. Geneva, CH, 2003. URL: <https://webstore.iec.ch/publication/6168#additionalinfo>.
- [6] Yong-Wook Kim. *Yong-Wook Kim's personal GitHub repository*. URL: <https://github.com/yongwookkkim/Theoretical-and-Experimental-Studies-of-Diffraction-on-Optical-Disks>.
- [7] Nina Sultanova, S. Kasarova, and I. Nikolov. "Dispersion Properties of Optical Polymers". In: *ACTA PHYSICA POLONICA A* 116 (Oct. 2009), pp. 585–587. DOI: [10.12693/APhysPolA.116.585](https://doi.org/10.12693/APhysPolA.116.585).

A Refractive Index of Polycarbonate Layer

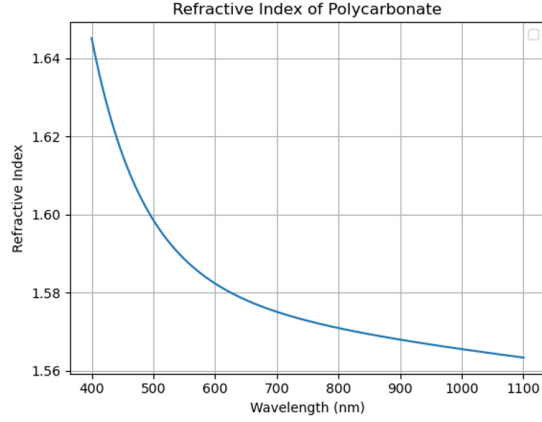


Figure 34: Fitted refractive index of polycarbonate as a function of wavelength.

The data from [7] was used to fit the refractive index of the polycarbonate cover layer as a function of wavelength. the resulting refractive index can be approximated by the formula:

$$n_{pc}(\lambda) = 1.51334706 + \frac{1.01457072 \times 10^2}{\lambda} - \frac{6.91264454 \times 10^4}{\lambda^2} + \frac{1.98566840 \times 10^7}{\lambda^3} \quad (18)$$

B Derivation of ΔOPL

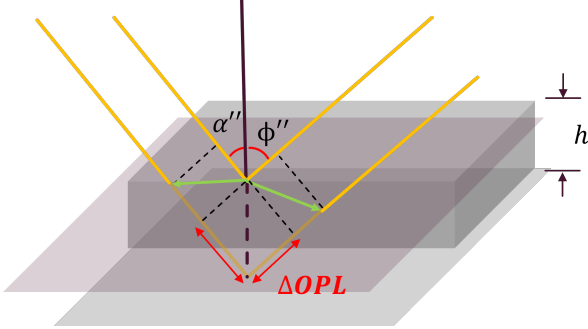


Figure 35: A schematic diagram of two parallel light rays that have the optical path difference ΔOPL .

In figure 35, $\sin \alpha''$ and $\sin \phi''$ are the angles that the light rays make with the normal after refraction by the polycarbonate layer. They satisfy Snell's Law: $n_{pc} \sin \alpha'' = \sin \alpha'$ and $n_{pc} \sin \phi'' = \sin \phi'$. ΔOPL is then the length the lower light ray traverses during the ascent/descent of height h , subtracted by the distance the upper ray travels parallel to it:

$$\Delta OPL = \frac{h}{\cos \alpha''} - h \tan \alpha'' \sin \alpha'' + \frac{h}{\cos \phi''} - h \tan \phi'' \sin \phi'' \quad (19)$$

Simplifying and substituting Snell's Law, we yield

$$\Delta OPL = \frac{h}{n_{pc}} \sqrt{n_{pc}^2 - \sin^2 \alpha'} + \frac{h}{n_{pc}} \sqrt{n_{pc}^2 - \sin^2 \phi'} \quad (20)$$

C Representing Track and Land as Convolutions

The data track is the sum of rectangle functions of length w along the x-axis.

$$\text{track} = \sum_n \text{rect}(x - n\Lambda, w) \quad (21)$$

Which can also be expressed as:

$$= \int_{-\infty}^{\infty} \text{rect}(u, w) \sum_n \delta(u - (x - n\Lambda)) du \quad (22)$$

Now, defining

$$g(x) = \sum_n \delta(x + n\Lambda) \quad (23)$$

the above integral can be rewritten as:

$$= \int_{-\infty}^{\infty} \text{rect}(u, w) g(u - x) du \quad (24)$$

which is the definition of a convolution.

$$\text{track} = \text{rect}(x, w) * g(x) \quad (25)$$

While the usual convolution notation would be written as $(f * g)(x)$, a different notation had been used for simplicity of calculation.

$$\text{track} = \text{rect}(x, w) * \sum_n \delta(x + n\Lambda) = \text{rect}(x, w) * \sum_n \delta(x - n\Lambda) \quad (26)$$

$x + n\Lambda$ and $x - n\Lambda$ can be interchanged because of the symmetry of the summation. The land can also be expressed as a convolution in a similar manner.

$$\text{land} = \text{rect}(x, w) * \sum_n \delta\left(x - n\Lambda - \frac{\Lambda}{2}\right) \quad (27)$$

D Computing the Fourier Integral for Simple Diffraction

We begin by evaluating the following integral.

$$\iint \text{rect}(x, w) * \sum_{n=-\frac{N}{2}}^{\frac{N}{2}-1} \delta(x - n\Lambda) e^{-i(\widetilde{k}_x x + \widetilde{k}_y y)} dx dy \quad (28)$$

Separating the variables:

$$\begin{aligned} & \iint \text{rect}(x, w) * \sum_{n=-\frac{N}{2}}^{\frac{N}{2}-1} \delta(x - n\Lambda) e^{-i(\widetilde{k}_x x + \widetilde{k}_y y)} dx dy \\ &= \int \text{rect}(x, w) * \sum_{n=-\frac{N}{2}}^{\frac{N}{2}-1} \delta(x - n\Lambda) e^{-i\widetilde{k}_x x} dx \int e^{-i\widetilde{k}_y y} dy \end{aligned} \quad (29)$$

Utilizing the convolution theorem for Fourier transforms, the integral can be further simplified to:

$$\begin{aligned}
& \int \text{rect}(x, w) * \sum_{n=-\frac{N}{2}}^{\frac{N}{2}-1} \delta(x - n\Lambda) e^{-i\tilde{k}_x x} dx \int e^{-i\tilde{k}_y y} dy \\
&= \int \text{rect}(x, w) e^{-i\tilde{k}_x x} dx \int \sum_{n=-\frac{N}{2}}^{\frac{N}{2}-1} \delta(x - n\Lambda) e^{-i\tilde{k}_x x} dx \int e^{-i\tilde{k}_y y} dy \quad (30)
\end{aligned}$$

It is well known that

$$\int \text{rect}(x, w) e^{-i\tilde{k}_x x} dx = w \text{sinc}\left(\tilde{k}_x \frac{w}{2}\right) \quad (31)$$

$$\begin{aligned}
& \int \sum_{n=-\frac{N}{2}}^{\frac{N}{2}-1} \delta(x - n\Lambda) e^{-i\tilde{k}_x x} dx = \sum_{n=-\frac{N}{2}}^{\frac{N}{2}-1} e^{-i\tilde{k}_x n\Lambda} = \frac{\sin\left(\frac{N}{2}\tilde{k}_x \Lambda\right)}{\sin\left(\frac{1}{2}\tilde{k}_x \Lambda\right)} e^{i\tilde{k}_x \frac{\Lambda}{2}} \\
& \int e^{-i\tilde{k}_y y} dy = 2\pi \delta\left(\tilde{k}_y\right) \quad (33)
\end{aligned}$$

Therefore, the integral in equation 28 is calculated to be

$$\iint \text{rect}(x, w) * \sum_{n=-\frac{N}{2}}^{\frac{N}{2}-1} \delta(x - n\Lambda) e^{-i(\tilde{k}_x x + \tilde{k}_y y)} dxdy = 2\pi w \text{sinc}\left(\tilde{k}_x \frac{w}{2}\right) \frac{\sin\left(\frac{N}{2}\tilde{k}_x \Lambda\right)}{\sin\left(\frac{1}{2}\tilde{k}_x \Lambda\right)} e^{i\frac{\tilde{k}_x}{2}\Lambda} \delta\left(\tilde{k}_y\right) \quad (34)$$

Now, using the definitions of track and land from 6, the observed complex amplitude, equation 7, may be written as:

$$\begin{aligned}
U &= U_o \iint \text{rect}(x, w) * \sum_{n=-\frac{N}{2}}^{\frac{N}{2}-1} \delta(x - n\Lambda) e^{-i(\tilde{k}_x x + \tilde{k}_y y)} dxdy \\
&+ U_o e^{in_{pc} k \Delta OPL} \iint \text{rect}(x, \Lambda - w) * \sum_{n=-\frac{N}{2}}^{\frac{N}{2}-1} \delta\left(x - n\Lambda - \frac{\Lambda}{2}\right) e^{-i(\tilde{k}_x x + \tilde{k}_y y)} dxdy \quad (35)
\end{aligned}$$

Using the results above and dropping the common factor of 2π , we compute the complex amplitude as:

$$\begin{aligned}
U &= U_o w \text{sinc}\left(\tilde{k}_x \frac{w}{2}\right) \frac{\sin\left(\frac{N}{2}\tilde{k}_x \Lambda\right)}{\sin\left(\frac{1}{2}\tilde{k}_x \Lambda\right)} e^{i\frac{\tilde{k}_x}{2}\Lambda} \delta\left(\tilde{k}_y\right) \\
&+ U_o e^{in_{pc} k \Delta OPL} (\Lambda - w) \text{sinc}\left(\tilde{k}_x \frac{(\Lambda - w)}{2}\right) \frac{\sin\left(\frac{N}{2}\tilde{k}_x \Lambda\right)}{\sin\left(\frac{1}{2}\tilde{k}_x \Lambda\right)} \delta\left(\tilde{k}_y\right) \quad (36)
\end{aligned}$$

Finally, computing $I = U\bar{U}$ yields:

$$\begin{aligned}
I &= |U_o|^2 \delta\left(\tilde{k}_y\right) \frac{\sin^2\left(\frac{N}{2}\tilde{k}_x \Lambda\right)}{\sin^2\left(\frac{1}{2}\tilde{k}_x \Lambda\right)} \left[w^2 \text{sinc}^2\left(\frac{1}{2}\tilde{k}_x w\right) + (\Lambda - w)^2 \text{sinc}^2\left(\frac{1}{2}\tilde{k}_x (\Lambda - w)\right) \right. \\
&\quad \left. + 2w(\Lambda - w) \text{sinc}^2\left(\frac{1}{2}\tilde{k}_x w\right) \text{sinc}^2\left(\frac{1}{2}\tilde{k}_x (\Lambda - w)\right) \cos\left(\frac{1}{2}\tilde{k}_x \Lambda - n_{pc} k \Delta OPL\right) \right] \quad (37)
\end{aligned}$$

Defining the terms in the square brackets $D(\alpha', \phi', \theta_o, \theta_s)$, we arrive at equation 8.

$$I = I_o \frac{\sin^2\left(\frac{N}{2}\widetilde{k}_x\Lambda\right)}{\sin^2\left(\frac{1}{2}\widetilde{k}_x\Lambda\right)} D(\alpha', \phi', \theta_o, \theta_s) \delta(\widetilde{k}_y)$$